Propagation of Acoustic-Gravity Waves in the Atmosphere[1]

FRANK PRESS AND DAVID HARKRIDER

Seismological Laboratory
California Institute of Technology, Pasadena

Abstract. Homogeneous wave guide theory is used to derive dispersion curves, vertical pressure distributions, and synthetic barograms for atmospheric waves. A complicated mode structure is found involving both gravity and acoustic waves. Various models of the atmosphere are studied to explore seasonal and geographic effects on pulse propagation. The influence of different zones in the atmosphere on the character of the barograms is studied. It is found that the first arriving waves are controlled by the properties of the lower atmospheric channel. Comparison of theoretical results and experimental data from large thermonuclear explosions is made in the time and frequency domains, and the following conclusions are reached: (1) The major features on barograms are due to dispersion; (2) superposition of several modes is needed to explain observed features; (3) scatter of data outside the range permitted by extreme atmospheric models shows the influence of winds for A_1; wind effects and higher modes are less important for A_2 waves. A discussion is included on atmospheric terminations and how these affect dispersion curves.

INTRODUCTION

Interest in the problem of the propagation of a pulse in the atmosphere began when world-wide pressure disturbances were observed in connection with the explosion of the volcano Krakatoa in 1883. The great Siberian meteorite of 1908 provided additional data which were used in attempts to correlate observations with theories of pulse propagation. These studies were prompted by a desire to account for the velocity of the pulse, to explain its peculiar signature, and to see if evidence could be found from progressive waves which would shed some light on the existence of free oscillations of the atmosphere. A mode of free oscillations having a period close to 12 solar hours is required by the resonance theory of the solar atmospheric tide. The atmospheric pulse was of further interest in that it could provide information concerning the structure of the atmosphere. (For a summary of early papers see *Wilkes* [1949].)

Interest in this problem was renewed with the detonation of thermonuclear bombs in the atmosphere. These 'megaton'-class explosions excited long atmospheric waves and provided data from a world-wide net of sensitive barographs [*Yamomoto,* 1956, 1957; *Hunt, Palmer, and Penney,* 1960; *Oksman and Katajo,* 1961; *Carpenter, Harwood, and Whiteside,* 1961; *Donn and Ewing,* 1961; *Wexler and Haas,* 1962]. Although the earlier theoretical studies [*Scorer,* 1950; *Pekeris,* 1948; *Yamomoto,* 1957] provided much insight into the nature of wave propagation, they were of limited use in analyzing the observations because these investigators were forced to assume oversimplified atmospheres in order to obtain solutions.

With the advent of the high-speed digital computer it became possible to obtain numerical solutions for a more realistic atmospheric model. In addition, the structure of the atmosphere is sufficiently well known from rocket soundings and satellite observations so that it is now not a significant variable of the problem. Major emphasis is therefore no longer placed on deducing the structure of the atmosphere, but on using a reasonably well known structure to explain the significant features observed on the barograms.

In this paper we present numerical solutions for the homogeneous problem of wave propagation in which the atmosphere is considered as a two-dimensional wave guide. Phase and group velocity dispersion curves and vertical pressure distributions are numerically evaluated for a number of modes and are discussed in terms of atmospheric structure. A comparison is made

[1] Contribution 1086, Division of Geological Sciences, California Institute of Technology.

between observations and theory in both the frequency and the time domain. The inhomogeneous problem, in which the source and atmospheric excitation functions are also included, will be treated in a following paper by the second author.

Our procedure will be to represent the complex vertical temperature structure of the atmosphere by a large number of isothermal layers. The solution to the equation of motion for each layer takes a particularly simple form. Boundary conditions at each interface and the characteristic equation for the multilayered wave guide are cast in a matrix formulation suggested by *Haskell* [1953] which is particularly suited for programming on a digital computer. In practice, 20 to 40 layers are sufficient to obtain an adequate approximation of the real atmosphere. This approach is similar to that of *Pfeffer and Zarichny* [1962], but our conclusions differ somewhat from theirs. *Yamomoto* [1957] and *Hunt, Palmer, and Penney* [1960] also used an isothermal layer representation, but they limited themselves to only a few layers. Although the latter authors were in error in their formulation of the interface boundary conditions, much of their discussion is still useful in elucidating the nature of the atmospheric pulse.

Theory and Numerical Methods

The linearized equations of motion for a constant velocity layer in a horizontally stratified atmosphere are given by [*Pekeris*, 1948][2]

$$\alpha_m^2\ddot{\chi}_m - \gamma g_m\dot{\chi}_m + \left[\omega^2 - k^2\alpha_m^2 + k^2(\gamma - 1)\frac{g_m^2}{\omega^2}\right]\chi_m = 0 \quad (1)$$

$$\delta_m w_m(z) = \omega^2\alpha_m^2\dot{\chi}_m + (g_m k^2\alpha_m^2 - g_m\gamma\omega^2)\chi_m \quad (2)$$

$$\delta_m p_m(z) = i\omega\rho_m^0(z) \cdot[-g_m\alpha_m^2\dot{\chi}_m + (\gamma g_m^2 - \omega^2\alpha_m^2)\chi_m] \quad (3)$$

$$\delta_m = g_m^2k^2 - \omega^4 \quad (4)$$

where the dots denote differentiation with respect to the vertical coordinate z. z is taken positive in the upward direction and a space and time dependence $J_0(kr)\exp(i\omega t)$ is included. Assuming azimuthal symmetry, χ_m is the first time derivative of the dilatation and is given in cylindrical coordinates by

$$\chi = \frac{\partial w}{\partial z} + \frac{1}{r}\frac{\partial(ru)}{\partial r} \quad (5)$$

where u, w, and p denote perturbations from equilibrium of horizontal velocity, vertical velocity, and pressure, respectively.

In addition, we have for the equilibrium state in each layer

$$\frac{dp^0}{dz} = -g\rho^0 \qquad p^0 = RK^0\rho^0$$

$$\alpha^2 = \gamma\frac{p^0}{\rho^0} = \gamma RK^0 \quad (6)$$

From (6) we obtain for layer m

$$\rho_m^0(z) = \rho_m^0(z_{m-1})e^{-2\lambda_m(z-z_{m-1})} = \rho_m^0 e^{-2\lambda_m(z-z_{m-1/2})}$$

where $\lambda_m = \gamma g_m/2\,\alpha_m^2$, $\rho_m^0 = \rho_m^0(z_{m-1/2})$, and $z_{m-1/2}$ is the altitude of the midpoint of the m layer. Since $p_m^0(z_{m-1}) = p_{m-1}^0(z_{m-1})$, we have

$$\frac{\rho_m^0(z_{m-1})}{\rho_{m-1}^0(z_{m-1})} = \frac{\alpha_{m-1}^2 p_m^0(z_{m-1})}{\alpha_m^2 p_{m-1}^0(z_{m-1})} = \frac{\alpha_{m-1}^2}{\alpha_m^2} \quad (7)$$

We assume small motions and impose the boundary conditions of continuity of vertical particle velocity and total pressure across the disturbed interfaces. Retaining only first-order terms, we find that the change in total pressure of a small parcel which is displaced a vertical distance η from its static equilibrium position z is the pressure perturbation, $p(z)$, at the zero displacement position plus $\delta p = -g\rho^0(z)\eta$. Now defining $p_P(z) = p(z) + \delta p$, using (3) and $w = i\omega\eta$, we obtain

$$p_{P_m}(z) = i\frac{\rho_m^0(z)}{\omega}\alpha_m^2\chi_m \quad (8)$$

At the layer interfaces we will now require

$$p_{P_{m-1}}(z_{m-1}) = p_{P_m}(z_{m-1})$$

in order to guarantee continuity of pressure. It is interesting to note that when there is no temperature or gravity discontinuity across an interface, one can use as a boundary condition

[2] For definitions of symbols not defined in the text, see appendix.

continuity of $p(z)$ since for that particular case $p_{P_m}(z_{m-1}) = p_{P_{m-1}}(z_{m-1})$ is equivalent to $p_m(z_{m-1}) = p_{m-1}(z_{m-1})$. This relation was used by *Pekeris* [1948] in his model of the atmosphere.

The general solution of (1) is given by

$$\chi_m = e^{\lambda_m z}[\Delta_m' e^{-ikr_{\alpha_m} z} + \Delta_m'' e^{ikr_{\alpha_m} z}] J_0(kr) e^{i\omega t} \tag{9}$$

where

$$kr_{\alpha_m} = \left[k^2\left(\frac{c^2}{\alpha_m^2} - 1\right) - \frac{\sigma_{Bm}^2}{c^2}\left(\frac{c^2}{\beta_m^2} - 1\right)\right]^{1/2} \tag{10}$$

for (c, k) such that $(kr_{\alpha_m})^2 > 0$, and

$$kr_{\alpha_m} = -i\left[k^2\left(1 - \frac{c^2}{\alpha_m^2}\right) - \frac{\sigma_{Bm}^2}{c^2}\left(1 - \frac{c^2}{\beta_m^2}\right)\right]^{1/2}$$

for (c, k) such that $(kr_{\alpha_m})^2 < 0$. Here $\beta_m = (2\sqrt{\gamma - 1}/\gamma)\alpha_m < \alpha_m$ for all $\gamma \geq 1$, and σ_{Bm} is the Brunt resonant angular frequency for the constant velocity layer m and is given by $\sigma_{Bm} = g_m\sqrt{\gamma - 1}/\alpha_m$.

Substituting (9) into (2) and (8), evaluating at z_m and z_{m-1}, and eliminating the constants Δ_m' and Δ_m'', we obtain the following matrix relation

$$\begin{bmatrix} w_m(z_m) \\ p_{P_m}(z_m) \end{bmatrix} = \begin{bmatrix} (a_m)_{11} & (a_m)_{12} \\ (a_m)_{21} & (a_m)_{22} \end{bmatrix} \begin{bmatrix} w_m(z_{m-1}) \\ p_{P_m}(z_{m-1}) \end{bmatrix} \tag{11}$$

where

$$(a_m)_{11} = e^{\lambda_m d_m} \cdot \left\{\cos P_m + \frac{g_m}{\alpha_m^2}\left(\frac{\alpha_m^2}{c^2} - \frac{\gamma}{2}\right)\frac{\sin P_m}{(kr_{\alpha_m})}\right\}$$

$$(a_m)_{12} = i(kc)^3 \cdot \frac{\left\{g_m^2\left(\frac{\alpha_m^2}{c^2} - \frac{\gamma}{2}\right)^2 + \alpha_m^4 (kr_{\alpha_m})^2\right\}}{\rho_m^0 \alpha_m^4 \delta_m}\frac{\sin P_m}{(kr_{\alpha_m})} \tag{12}$$

$$(a_m)_{21} = i\,\frac{\rho_m^0 \delta_m}{(kc)^3}\frac{\sin P_m}{(kr_{\alpha_m})}$$

$$(a_m)_{22} = e^{-\lambda_m d_m} \cdot \left\{\cos P_m - \frac{g_m}{\alpha_m^2}\left(\frac{\alpha_m^2}{c^2} - \frac{\gamma}{2}\right)\frac{\sin P_m}{(kr_{\alpha_m})}\right\}$$

and $P_m = (kr_{\alpha_m})\, d_m$. In equations 12 we see that matrix elements $(a_m)_{jk}$ are real or imaginary for (c, k) real and for $j + k$ equal to even or odd integers, respectively. Therefore, the elements of a matrix resulting from the matrix multiplication of any number of layer matrices will be real or imaginary in the same sense as the individual matrices.

For $g_m = 0$ the a_m matrix reduces to a form equivalent to the nongravitating liquid-layer matrix given by *Dorman* [1962] in his discussion of elastic wave propagation in layered wave guides.

The conditions for continuity of w and p_P at interfaces and the connection between layers described by (11) together enable us to write the following matrix relation

$$\begin{bmatrix} w_{n-1}(z_{n-1}) \\ p_{P_{n-1}}(z_{n-1}) \end{bmatrix} = A \begin{bmatrix} w_0(0) \\ p_{P_0}(0) \end{bmatrix} \tag{13}$$

where $A = a_{n-1} \cdots a_1$.

At $z = 0$, layer 1 is in contact with a flat rigid boundary where we require $w_0(0) = 0$ and thus $p_{P_0}(0) = p_0(0) \equiv p_0$. Equation 13 becomes

$$\begin{bmatrix} w_{n-1}(z_{n-1}) \\ p_{Pn-1}(z_{n-1}) \end{bmatrix} = A \begin{bmatrix} 0 \\ p_0 \end{bmatrix} \tag{14}$$

Before deriving the period equation for an atmosphere terminated by an isothermal half-space extending from z_{n-1} to infinity, we consider two special cases.

The first is an atmosphere bounded at z_{n-1} by a free surface. For this case we have $p_{P_{n-1}}(z_{n-1}) = 0$, and (14) reduces to

$$\begin{bmatrix} w_{n-1}(z_{n-1}) \\ 0 \end{bmatrix} = A \begin{bmatrix} 0 \\ p_0 \end{bmatrix}$$

which in turn yields $A_{22}\, p_0 = 0$. Therefore, the period equation for an atmosphere with a free surface at z_{n-1} is

$$A_{22} = 0 \tag{16}$$

The second case is an atmosphere bounded by a rigid surface at z_{n-1}. Here we have $w_{n-1}(z_{n-1}) = 0$, and (14) reduces to

$$\begin{bmatrix} 0 \\ p_{P_{n-1}}(z_{n-1}) \end{bmatrix} = A \begin{bmatrix} 0 \\ p_0 \end{bmatrix}$$

which yields the following period equation:

$$A_{12}^* = 0 \tag{17}$$

where $iA_{jk}^* = A_{jk}$ and A_{jk}^* is real for $j + k$ equal to an odd integer.

For the case of an atmosphere bounded by an isothermal half-space, we require that the nth layer coefficient $\Delta_n'' = 0$. For $(kr_{\alpha n})^2 > 0$ this is equivalent to requiring that there be no radiation from infinity into the wave guide. For $(kr_{\alpha n})^2 < 0$ this requirement guarantees that the kinetic energy integrated over a column of atmosphere will be finite.

Setting $\Delta_n'' = 0$ in the solution for $w_n(z)$ and $p_{P_n}(z)$ evaluated at z_{n-1} we find that

$$\begin{bmatrix} w_{n-1}(z_{n-1}) \\ p_{P_{n-1}}(z_{n-1}) \end{bmatrix} = \begin{bmatrix} w_n(z_{n-1}) \\ p_{P_n}(z_{n-1}) \end{bmatrix} = \Delta_n' \begin{bmatrix} b_{1n} \\ b_{2n} \end{bmatrix} \tag{18}$$

where

$$b_{1n} = \frac{e^{\lambda_n z_{n-1}}}{\delta_n} e^{-ikr_{\alpha_n} z_{n-1}} (kc)^2 \cdot \left\{ g_n \left(\frac{\alpha_n^2}{c^2} - \frac{\gamma}{2} \right) - i\alpha_n^2 (kr_{\alpha_n}) \right\} J_0(kr) e^{i\omega t} \tag{19}$$

$$b_{2n} = i \frac{e^{\lambda_n z_{n-1}}}{\delta_n} e^{-ikr_{\alpha_n} z_{n-1}} (kc)^2 \cdot \frac{\rho_n^0(z_{n-1})\alpha_n^2}{(kc)^3} \delta_n J_0(kr) e^{i\omega t}$$

Substituting (18) into (14) and eliminating Δ_n' from the two resulting linear equations, we obtain as the period equation for an n layered half-space

$$A_{12} - \frac{b_{1n}}{b_{2n}} A_{22} = 0$$

or

$$A_{12}^* + (kc)^3 \frac{\left[g_n \left(\frac{\alpha_n^2}{c^2} - \frac{\gamma}{2} \right) - i\alpha_n^2 (kr_{\alpha_n}) \right]}{\rho_n^0(z_{n-1})\alpha_n^2 \delta_n} \cdot A_{22} = 0 \tag{20}$$

All quantities in (20) are always real for all (c, k) real except for $i(kr_{\alpha_n})$, which is real or imaginary depending on the values of the real (c, k). Since in this paper we are interested in undamped propagation, we now make the requirement that $(kr_{\alpha_n})^2$ be negative. This excludes leaking or complex modes of propagation. Under this condition, (20) is real and takes the form used in numerical calculation of dispersion curves:

$$A_{12}^* + (kc)^3 \frac{\left[g_n \left(\frac{\alpha_n^2}{c^2} - \frac{\gamma}{2} \right) - \alpha_n^2 |kr_{\alpha_n}| \right]}{\rho_n^0(z_{n-1})\alpha_n^2 \delta_n} \cdot A_{22} = 0 \tag{21}$$

The condition that $(kr_{\alpha_n})^2$ be negative now prescribes a cutoff region in the (c, k) plane defined by $(kr_{\alpha_n}) = 0$. The boundary of this region is obtained in terms of c and period T by setting (10) equal to zero. This yields

$$T = T_{Bn} \left(\frac{c^2}{\alpha_n^2} - 1 \right)^{1/2} \Big/ \left(\frac{c^2}{\beta_n^2} - 1 \right)^{1/2} \tag{22}$$

where T_{Bn} is the Brunt resonant period of the half-space and is given by $T_{Bn} = 2\pi/\sigma_{Bn}$. From (22) we have the following asymptotic values of the boundaries of the cutoff region:

$$\begin{aligned} T &\to \left(\frac{\beta_n}{\alpha_n} \right) T_{Bn} \quad \text{for} \quad c \to \infty \\ T &= 0 \quad \text{for} \quad c = \alpha_n \\ &\text{No cutoff region for} \quad \beta_n \le c \le \alpha_n \\ T &\to \infty \quad \text{for} \quad c \to \beta_n \\ T &= T_{Bn} \quad \text{for} \quad c = 0 \\ &\text{No cutoff region for} \quad \left(\frac{\beta_n}{\alpha_n} \right) T_{Bn} \le T \le T_{Bn} \end{aligned} \tag{23}$$

In deriving (13) we have as a by-product the following matrix relation

$$\begin{bmatrix} w_m(z_m) \\ p_{Pm}(z_m) \end{bmatrix} = A_m \begin{bmatrix} 0 \\ p_0 \end{bmatrix} \tag{24}$$

where $A_m = a_m \cdots a_1$

Furthermore, at the layer midpoints, $z_{m-1/2}$, it can easily be shown that

$$\begin{bmatrix} w_m(z_{m-1/2}) \\ p_{Pm}(z_{m-1/2}) \end{bmatrix} = A_{m-1/2} \begin{bmatrix} 0 \\ p_0 \end{bmatrix} \tag{25}$$

where $A_{m-1/2} = a_{m-1/2} a_{m-1} \cdots a_1$ and $a_{m-1/2}$ is of the same form as a_m with d_m replaced by $d_{m-1/2} = d_m/2$ and all other quantities remain unchanged.

Rewriting (25) we obtain

$$\frac{w_m^*(z_{m-1/2})}{p_0} = (A_{m-1/2})_{12}^* \tag{26}$$

where $w = iw^*$ and $p_{P_m}(z_{m-1/2})/p_0 = (A_{m1/2})_{12}$.

From the definition of p_{P_m} we have

$$\frac{p_m(z_{m-1/2})}{p_0} = (A_{m-1/2})_{22} + \frac{\rho_m^0 g_m}{(kc)} (A_{m-1/2})_{12}^* \tag{27}$$

Now defining the r-independent part of $p_m(z, r)$ as $\bar{p}_m(z)$ or $p_m(z, r) = \bar{p}_m(z) J_0(kr)$, and since

$$u_m(z, r) = i \frac{1}{\omega \rho_m^0(z)} \frac{\partial p_m(z, r)}{\partial r}$$

we obtain

$$\frac{\bar{u}_m^*(z_{m-1/2})}{\bar{p}_0} = -\frac{1}{c\rho_m^0} \cdot \left[(A_{m-1/2})_{22} + \frac{\rho_m^0 g_m}{(kc)} (A_{m-1/2})_{12}^* \right] \tag{28}$$

where $u_m(z, r) = i \bar{u}_m^*(z) J_1(kr)$.

The normalized particle velocities and pressures are given in (26) to (28) at the layer midpoints rather than at the layer boundaries in order to make them correspond more closely to the smooth distribution in nature.

The matrix formulation described above is very convenient for numerical calculations; it was first used for earthquake surface waves by *Haskell* [1953]. For our computations we programmed the dispersion calculation for an IBM 7090 computer. This program was written in Fortran and used for production runs. As an independent check on the program, we also wrote a program for our small computer, the Bendix G-15D. The Fortran program has the option of calculating the three models for terminating the atmosphere discussed above for any given layering of the atmosphere.

The general computational procedure is to find the zeros of a function F of phase velocity, wave number, and the physical constants of the layers. For an atmosphere bounded by an isothermal half-space, the F function is defined as the left-hand side of (21); for an atmosphere bounded by a free surface, the left-hand side of (16); and for an atmosphere bounded by a rigid surface, the left-hand side of (17).

The flow of the program is similar to that in the programs described by *Press, Harkrider, and Seafeldt* [1961] and *Harkrider and Anderson* [1962]. The zeros of F are determined by initially specifying the phase velocity c and a trial value of the wave number k. The elements of the a_m matrix are formed at each layer and then multiplied by the matrix of the layer above it, starting with the layer at the surface. After the matrix product for all layers has been calculated, the program then combines these numerical quantities to obtain a value for F. New trial values of k (of increasing or decreasing size depending on the sign of the initial F value) specified by an input Δk are used to calculate new F values until the root is bracketed by a change of sign in F. Linear interpolation and extrapolation are then repeatedly used to find small F values until k's of different F sign are within the precision interval desired. The resulting interpolated value of k is the output value given as the root for the input c.

The program has an additional feature in that, as an input option, the first or second roots (two smallest k roots) will be found for a given c. This is accomplished by starting at the smallest k outside the cutoff region (F complex) and finding either the first or second sign change of F. The roots associated with either mode are then computed. For all values of c in the free and rigid surface models and for $c \geq \beta_n$ in the isothermal half-space model, this initial k is zero. For $c < \beta_n$ in the isothermal half-space model, the initial k is determined by (22).

In all models calculated we found that each continuous dispersion curve or mode was a monotonic decreasing function of c versus k or T and always had the same sign change in F through the root region. This made it easy to track all the roots of a preselected mode. To save computer time and to keep from jumping modes, the k root for the previous c is used as the starting point for the new c. Further details about root hunting procedures can be found in papers by *Press et al.* [1961] and *Harkrider and Anderson* [1962].

Once a root is found by the computer, the velocity and pressure ratios given by (26), (27), and (28) are calculated at the midpoint in each layer. The vertical distribution of these ratios is generally diagnostic of the particular mode and provides a check against mode jumping. The group velocity is computed by numerical differentiation of the phase velocity values. $\Delta c/\Delta k$ is obtained by perturbing c slightly and then finding a new k root.

The program has two options for input of layer constants. The first reads d_m and K_m^0 from

data cards. From (6) and (7) we then calculate α_m and ρ_m^0, where for calculation purposes ρ_m^0 is given by

$$\rho_m^0 = \rho_0^0 \frac{K_0^0}{K_m^0} \exp\left(-\sum_{i=1}^{m-1} 2\lambda_i d_i - \lambda_m d_m\right) \quad (29)$$

Here ρ_0^0 and K_0^0 are the equilibrium values for surface density and temperature, respectively. The second input option is to read in d_m, α_m, and ρ_m^0 directly.

From (7) we see that in order to obtain λ_m and in turn (29), we must calculate the layer gravity g_m. In the cases given in this paper the constant gravity in layer m, g_m, was chosen to be the value of gravity for a spherical earth at an altitude equal to the layer midpoint $z_{m-1/2}$.

As in previous programs, numbers of the order of exp $(k \sum_{i=1}^{n-1} d_i)$ are involved in the calculation of F. Therefore, as c decreases and k increases, the larger root values of k will lead to machine overflow, if the total number of layers remains constant. When this occurs, the program will automatically reduce layers starting at high altitudes until F no longer overflows. The program then recalculates the root for the previous larger c in order to verify that no loss in precision of the k root was caused by layer reduction.

It can be shown that the determinants of the a_m matrices are identically equal to unity for all values of (c, k). It follows that the determinant of the product matrix A is also equal to 1. Therefore, if loss in significance occurs owing to machine round-off during the matrix multiplication loop, the numerical values of the product matrix determinant will differ greatly from 1. As a check on the validity of roots, the program calculates and prints this determinant for each root.

From (12) we see that certain matrix elements are infinite at $\delta_m = 0$. For each layer, $\delta_m = 0$ defines a straight line in the (c, T) plane given by $T_m = 2\pi c/g_m$. Since $g_0 \geq g_m \geq g_n$, the vanishing δ_m's for all layers fall in the region bounded by $T = 2\pi c/g_0$ and $T = 2\pi c/g_n$. This region will be shown on the dispersion curve figures as a stippled wedge starting at $(c, T) = (0, 0)$ and extending to the top of the figures. To keep the programs from needlessly reducing layers due to overflow caused by a trial k being close to the zeros of δ_m, the computation is programmed to keep c and k out of this region.

As checks on our procedures, we calculated several asymptotic expressions for comparison with well-known equations. For example, our formulas reduce to those for sound waves in layered nongravitating liquids and to gravity waves in an incompressible ocean over a rigid bottom. They also yield the period equation for internal gravity waves between two incompressible liquids.

Digital Models of the Atmosphere

Figure 1 shows the manner in which several model atmospheres were represented by isothermal layers. The standard ARDC atmosphere [*Wares, Champion, Pond, and Cole,* 1960], which combines data from all sources, is used as our basic model. It is represented by a digital model with 39 layers and is terminated with an isothermal half-space beginning at an elevation of 220 km. Also shown are the following models: an atmosphere terminated with an isothermal half-space at 108 km; atmospheres terminated with rigid and free surfaces at 220 km. Not shown but also studied were several models with half-spaces beginning between 108 and 220 km. These models are studied to see how the dispersion curves and consequently the theoretical

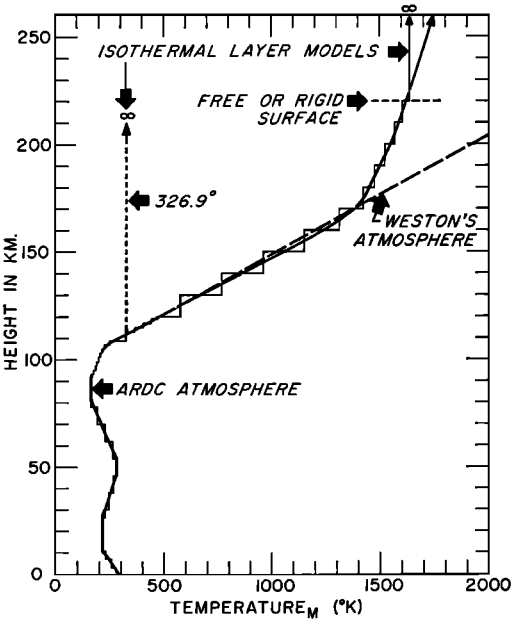

Fig. 1. ARDC standard atmosphere and its approximation by isothermal layers.

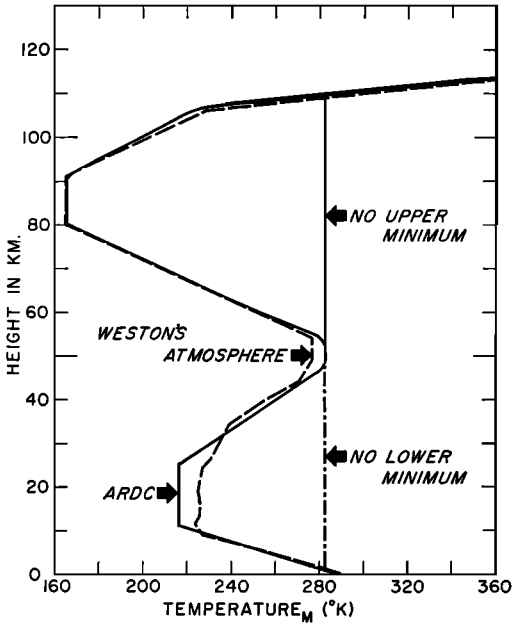

Fig. 2. Modifications to the standard atmosphere made in order to study the effect of different zones.

barograms are affected by the manner in which the atmosphere is terminated. *Weston's* [1961] model in which the atmosphere is terminated by a half-space with linear temperature gradient is also shown.

Figure 2 shows the ARDC atmosphere together with several modifications for which dispersion curves were also computed. These models were designed to study the influence of different regions of the atmosphere on the character of the disturbance. Thus the effect of the upper or lower channel is studied separately by removing these channels entirely, leaving the remaining portions untouched.

To explore seasonal and geographic influences we use other ARDC models as shown in Figure 3. We might expect that the models for the arctic winter and tropical atmospheres represent the limits within which the observations should fall in the absence of wind effects. These extreme atmospheres were defined to 30 km only. Above these elevations we have arbitrarily forced them to join the standard ARDC curve.

Dispersion Curves

In this section we discuss the dispersion curves for the various model atmospheres. Phase and group velocity curves are presented as a function of period for several modes of propagation. These curves may be compared with observational data in two ways. Group velocity data are obtainable from single barograms and can be compared directly with these curves. Phase velocity data may be derived in principle from an array of at least three stations or from a single station if the initial phase at the source is known. Experimental phase velocities are not yet available, however. The theoretical curves may be used to predict the sequence of wave arrivals in the time domain. This can be done qualitatively by interpreting the ordinate of the group velocity curve as being proportional to the reciprocal travel time. It can be done more realistically by using phase and group velocity curves in a Fourier synthesis to obtain a synthetic barogram. Both methods will be tried in a later section.

ARDC standard without gravity. This model was designed to enable us to examine the role of gravity in the propagation of atmospheric waves. By reducing gravity to negligibly small values in equation 21, we obtained the dispersion curves of Figure 4 for a nongravitating ARDC standard atmosphere. The gravest acoustic mode S_0 and the first acoustic mode S_1 of the

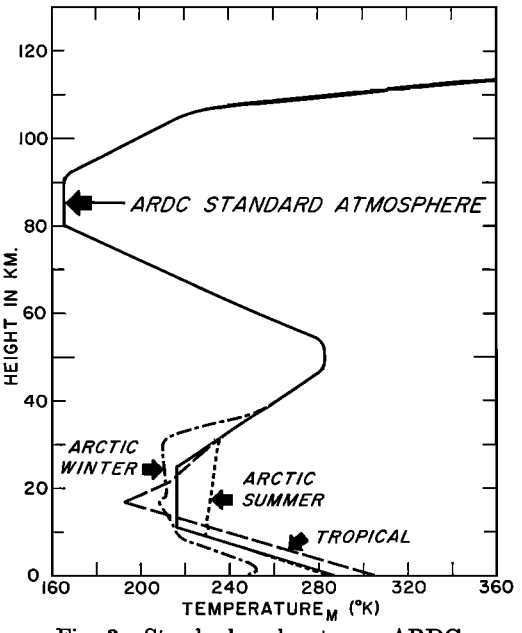

Fig. 3. Standard and extreme ARDC atmospheres.

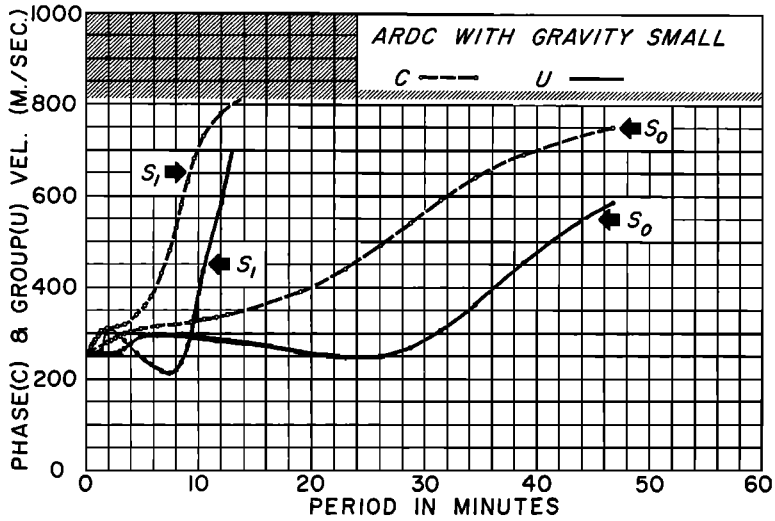

Fig. 4. Phase and group velocity dispersion curves for S_0 and S_1 modes of nongravitating ARDC standard atmosphere with half-space beginning at 220 km.

infinite set of modes are plotted. Both exhibit a general feature of acoustic wave guides in that the high-frequency limit of phase and group velocity of all modes is the sound velocity in the channel with smallest velocity. In our case, this is the second minimum temperature zone at 85 km. In the S_0 mode, phase and group velocities approach the velocity in the half-space at infinitely long periods. If the lower boundary were free rather than rigid, a finite long-period cutoff period would occur. Two minimal values of group velocity occur at 2 minutes and 23 minutes and a maximum value occurs at 6 to 7 minutes. From the S_0 curve we would expect a transient arrival (T approximately 6 to 7 min) at a time corresponding to the group velocity maximum of 297 m/sec. This would be followed by waves showing both direct

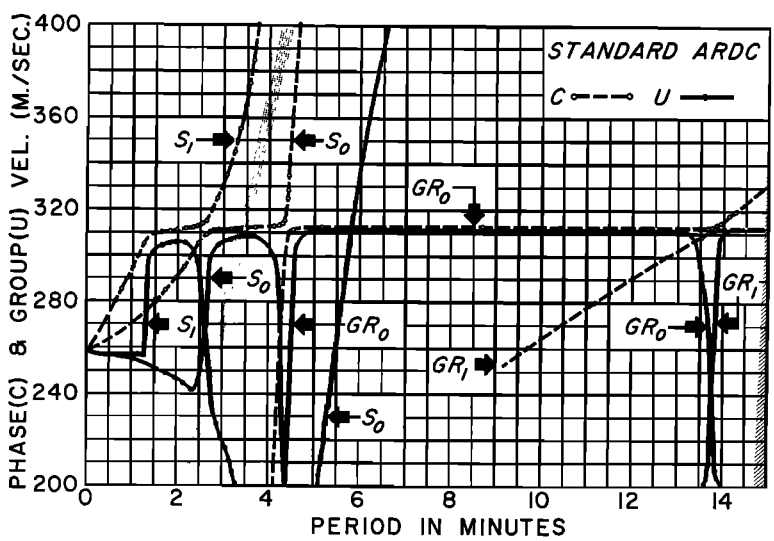

Fig. 5. Phase and group velocity dispersion curves for $S_{0,1}$ and $GR_{0,1}$ modes of ARDC standard atmosphere with half-space beginning at 220 km. Strippling indicates region where singular values of F occur. Cutoffs are indicated by hatched region.

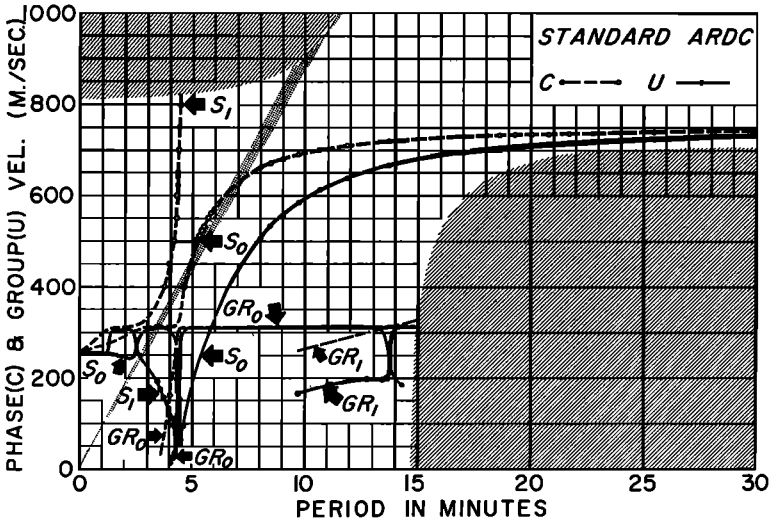

Fig. 6. Same as Figure 5 with different scale.

and inverse dispersion. Longer waves (T approximately 30 min) would arrive earlier, but we will raise doubts in the next section as to whether these waves would be observed. The homogeneous wave-guide theory cannot predict relative amplitudes but only possible modes of propagation. It is interesting that in a general way the nongravitating atmosphere predicts a barogram not unlike that which is observed. Gravity changes the shape of the group velocity curve somewhat; it increases the maximum group velocity of those waves having periods of 6 to 7 minutes by about 5 per cent and introduces new modes whose excitation by near-surface nuclear explosions is probably small.

The higher mode S_1 has a cutoff period at about 14 minutes where phase and group velocity reach the half-space velocity of sound. One can infer the dispersive (but not the amplitude) properties of propagation according to this mode in a manner similar to that for S_0.

ARDC standard atmosphere. Dispersion

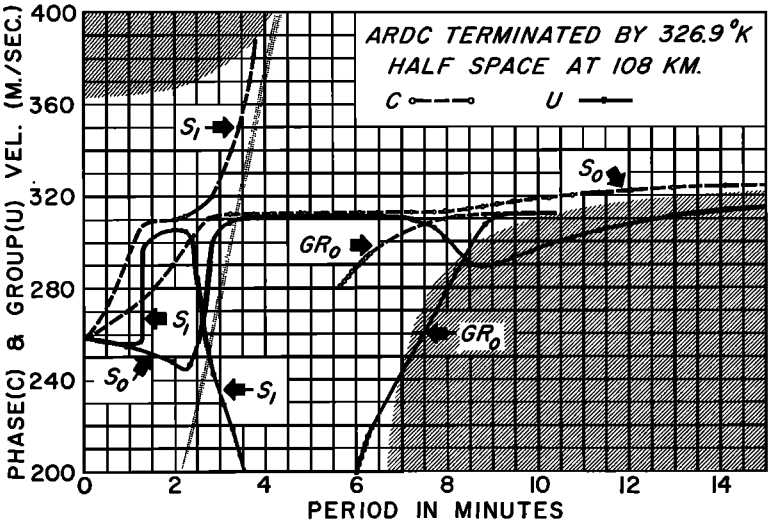

Fig. 7. Phase and group velocity dispersion curves for $S_{0,1}$ and GR_0 modes of ARDC standard atmosphere with half-space beginning at 108 km.

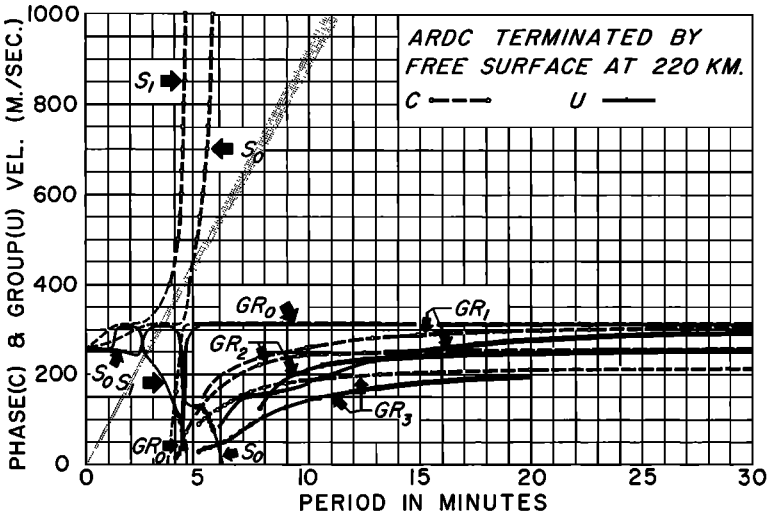

Fig. 8. Phase and group velocity dispersion curves for $S_{0,1}$ and $GR_{0,1,2,3}$ modes of ARDC standard atmosphere with free surface at 220 km.

curves are plotted in Figures 5 and 6 for the ARDC atmosphere terminated with an isothermal half-space at 220 km. Figure 7 shows the curves for the same model terminated with a lower-temperature half-space at 108 km. Figures 8 and 9 show dispersion curves for this model terminated with a free and a rigid surface, respectively, at 220 km. The hatched areas in the upper half and the lower right portions of Figures 5 to 7 are the cutoff regions within which lossless propagation does not occur because of radiation into the half-space. Radiation losses do not occur for the models with free and rigid surface terminations. The oblique stippled band represents a region of singular values of F corresponding to $\delta_m = 0$. The program omits these regions.

The dispersion curves are separated into modes S_0 and S_1, GR_0 and GR_1. The S modes are the first two of an infinite set, analogous to the corresponding acoustic modes of the non-gravitating model. This correspondence is based

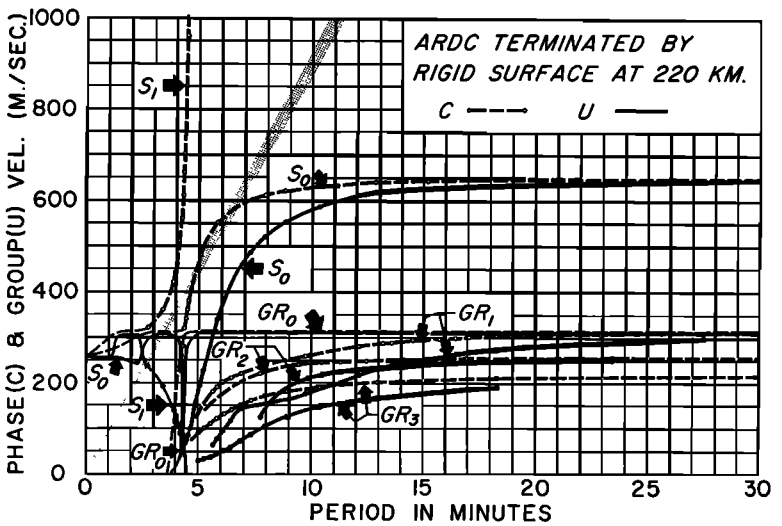

Fig. 9. Phase and group velocity dispersion curves for $S_{0,1}$ and $GR_{0,1,2,3}$ modes of ARDC standard atmosphere with rigid boundary at 220 km.

on the similarity in dispersion curves for T less than 4 minutes; it also follows from the fact that in both cases the pressure-height curve has no nodes for S_0 and one node for S_1.

The high-frequency limit of the S_0 and S_1 curves is the sound velocity in the upper channel. At infinite period, phase and group velocities of S_0 reach values of about 0.75 km/sec. S_1 has a long-period cutoff near 4 minutes, with limiting phase and group velocities somewhat higher than the half-space sound velocity (Figures 5 to 7). For the free surface model (Figure 8), S_0 and S_1 approach infinite phase velocities and zero group velocities at long-period cutoffs. This is also true for S_1 in the model with rigid upper boundary. However, S_0 for this case is characterized by a phase and group velocity which reaches 0.65 km/sec at infinite period.

The modes GR_0 and GR_1 are not present for the nongravitating model. We shall see later that GR_0 is characterized by vertical particle displacement with no nodes, GR_1 has one node, etc. A large number of GR modes has been found, but only a few are plotted. It is unusual that with increasing mode number (as defined by an increasing number of nodal surfaces) the period increases. With decreasing period the GR modes are characterized by phase and group velocities that reach zero. For increasing periods, phase velocity curves run into cutoffs for the half-space models. Group velocity maximums for GR_0 and GR_1 form flat plateaus at 312 m/sec. For the models with free and rigid surface terminations phase and group velocity for the GR modes have no long-period cutoffs. GR_0 shows the same plateau in group velocity at 312 m/sec. The higher GR modes have plateaus below this. Dispersion curves corresponding to GR modes were first shown by *Gazaryan* [1961].

These four variations of the ARDC model are studied to determine the effect on the dispersion curve of the method of termination of the atmosphere. All models have the following features in common: (1) phase and group velocities are essentially the same for S_0 and S_1 modes for periods less than about 3¾ and 3 minutes, respectively; (2) between 5 and 15 minutes broad flat maximums in group velocity occur in the S_0 and GR modes, all with the value of 312 m/sec. The curves for the various models differ for periods greater than 3 to 3¾ minutes in the regions of steeply rising phase and group velocity. These portions of the dispersion curves are sensitive to the precise manner in which the very low density atmosphere above 100 km is specified.[3] We would expect therefore that the corresponding waves are not likely to be excited by near-ground explosions

[3] From studies of other cases we find that, for termination of the atmosphere above 150 km, the steep portions of the S_0 and GR_0 curves are the same for T less than 13 min for these four variations of the ARDC model.

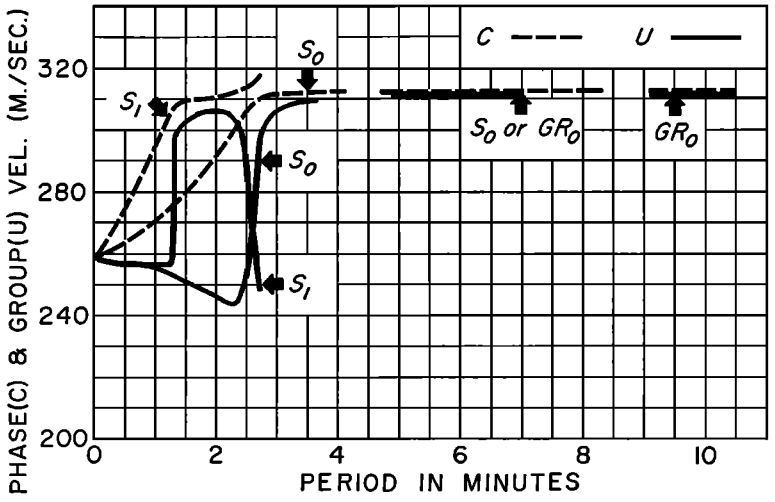

Fig. 10. Pseudo-dispersion curve formed from segments of ARDC models in Figures 5 to 9 which are identical.

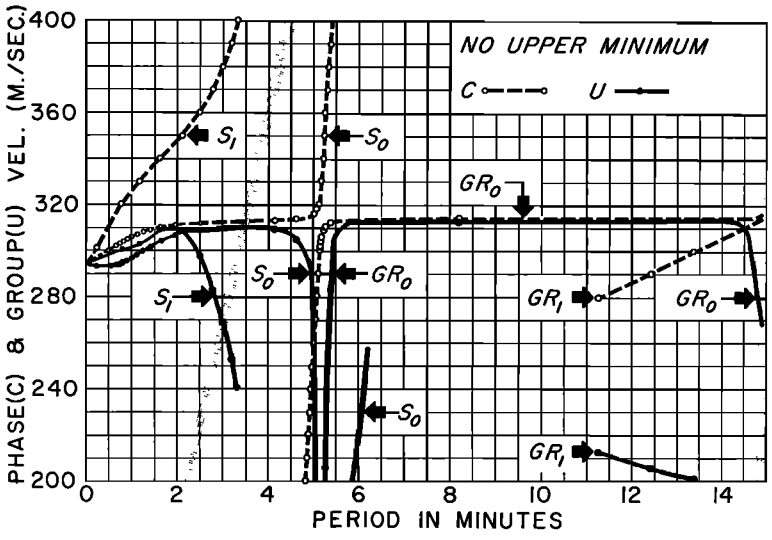

Fig. 11. Dispersion curves for modified ARDC model with no upper temperature minimum.

recorded by ground based detectors. Since amplitudes are proportional to $(dU/dT)^{-1/2}$, there is further reason to expect relatively small values for the excitation function of these waves.

The invariant portions of the dispersion curves for these ARDC standard models are reproduced in Figure 10. We would expect that most of the energy excited by near-surface explosions propagates according to these values of phase and group velocity. The first-arriving waves would correspond to the region of flat group velocity curves for the S_0 and GR modes. Thus a transient containing periods of 3 to 10 minutes would arrive at a time corresponding to a propagation velocity of 312 m/sec. This would be followed by waves of gradually decreasing period. At a time corresponding to propagation with a velocity of 305 m/sec waves with periods of 1½ to 2½ minutes would become significant. These are associated with the maximum group velocity of the S_1 mode and would be superposed on the S_0 and GR oscillations. The following oscillations would be complicated because they would result from a superposition of these and

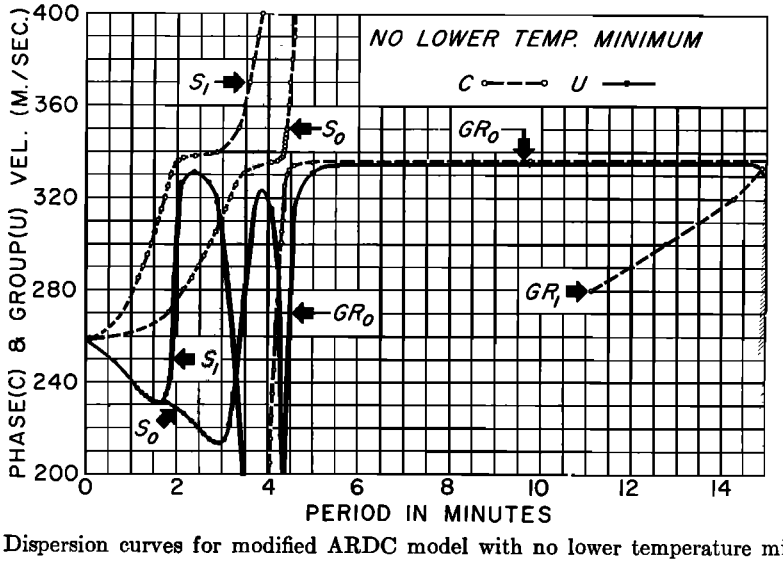

Fig. 12. Dispersion curves for modified ARDC model with no lower temperature minimum

higher modes. Until the excitation functions for the several modes have been computed, it will be difficult to determine the energy distribution with a single mode and among the various modes. We shall see that the minimum group velocity in S_0 at 2.4 minutes is sensitive to the properties of the upper channel. Whether waves corresponding to this part of the dispersion curve can be excited by near-surface explosions is questionable. We note also that although inverse dispersion is predicted in some of the models its form also depends on the properties of the atmosphere above 100 km. We would expect that long, inversely dispersed waves should be weakly excited by near-surface explosions. If such waves are observed, they would be particularly useful in inferring the manner in which the upper-atmosphere termination takes place.

Oksman and Kataja [1961] report disturbance of the ionosphere (revealed by vertical-incidence ionosonde) which occurred before the arrival of pressure waves. These may correspond to the long-period waves in the S_0 mode having group velocities between 0.312 and 0.75 km/sec (Figure 6) which are sensitive to the properties of the atmosphere above 100 km. However, hydromagnetic effects, not considered here, would probably play an important role in determining the character of these waves.

Weston [1961] raises certain objections to isothermal layer models. He points out that, despite the fact that the energy is bounded, the particle motions diverge with increasing elevation in the half-space, thus violating the small-motion assumption. By exploring various methods of terminating the atmosphere, some of which do not contain half-spaces, we have found major segments of dispersion curves which are independent of the atmosphere above about 100 km. It seems reasonable to conclude that these invariant values of phase and group velocity are appropriate for near-surface explosions and detectors.

It is interesting that flat segments of phase and group velocity of S_1, S_0, GR_0, and GR_1 are nearly connected to form a common dispersion curve. The steep segments of the dispersion curves are similarly related. The character of the propagating disturbance at any time is perhaps better represented by pseudo dispersion curves formed from segments of several modes. The segments which form a pseudo mode are all particularly sensitive to a given region of the wave guide. It will be shown that in the sequence of maximums in group velocity all are associated with the properties of the lower channel of the atmosphere. This phenomenon has also been observed for multilayered elastic wave guides [*Tolstoy*, 1959].

ARDC—no upper minimum. This model (Figures 2 and 11) was studied to see how the upper channel of the atmosphere affects the dispersion curve. The major changes which occur are: (1) very-short-period energy now travels

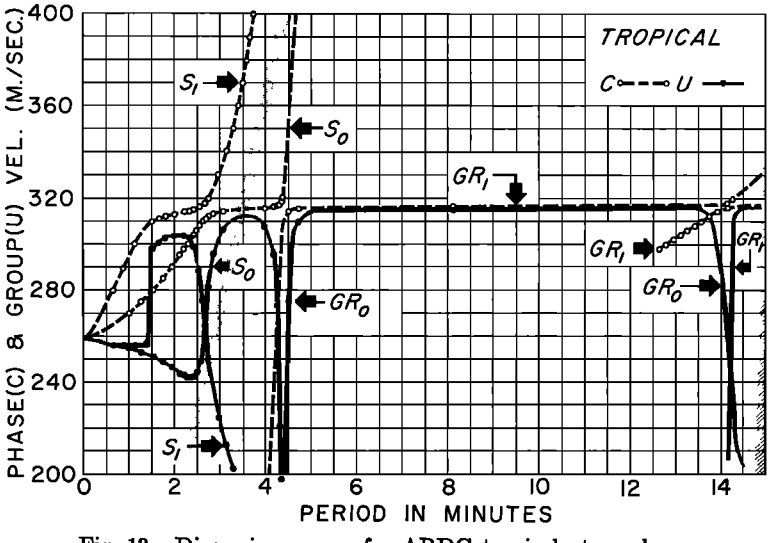

Fig. 13. Dispersion curves for ARDC tropical atmosphere.

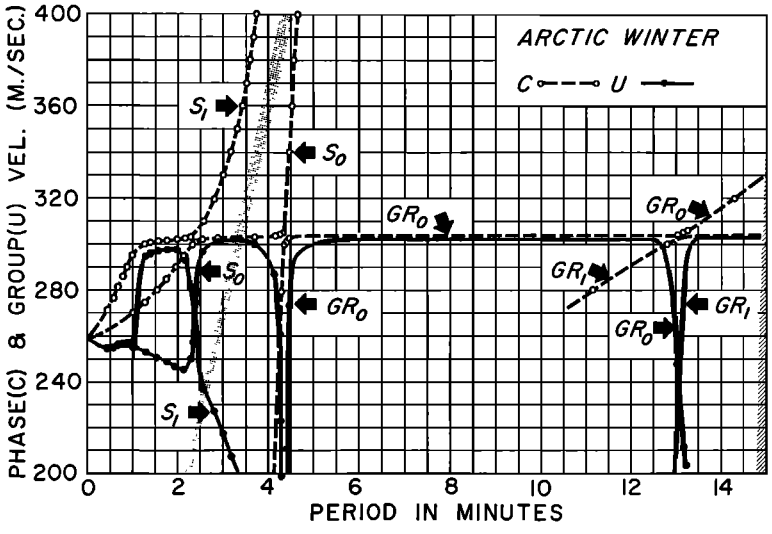

Fig. 14. Dispersion curves for ARDC arctic winter atmosphere.

with sound velocity in the lower channel; (2) the minimums in group velocity for the S_0 and S_1 modes shown in Figure 5 almost disappear. The time of arrival of the first waves, corresponding to the group velocity maximums of GR_1, S_0, and S_1, is almost unchanged and is therefore unaffected by the properties of the atmosphere above 50 km.

ARDC—no lower minimum. This model (Figures 2 and 12) demonstrates that the arrival time of the first waves is particularly sensitive to the properties of the lower atmospheric channel which occupies the region between 0 and 50 km. The maximums in group velocity associated with the first waves are shifted from 305 to 312 m/sec to 320 to 335 m/sec. GR_0 and GR_1 are otherwise unchanged. The minimums in group velocity of S_0 and S_1 are deepened, but the short-period limit of phase and group velocity is unchanged.

ARDC seasonal and geographic models. Results for ARDC models of tropical, arctic win-

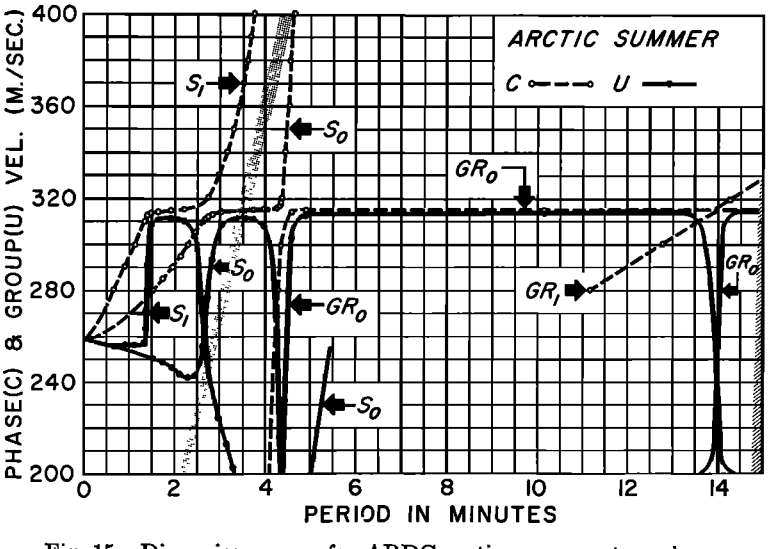

Fig. 15. Dispersion curves for ARDC arctic summer atmosphere.

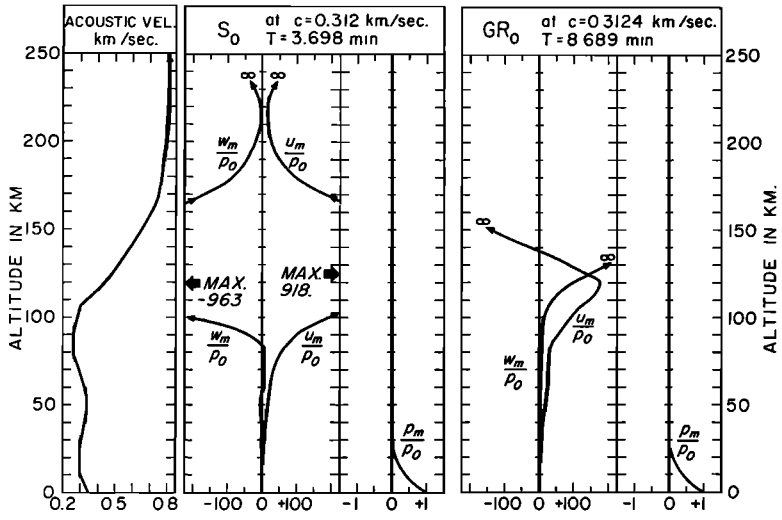

Fig. 16. Vertical distribution of normalized particle velocities and pressure for S_0, GR_0.

ter, and arctic summer atmospheres (Figure 3) are presented in Figures 13 to 15. In these models the properties of the atmosphere below 40 or 50 km are varied. As might be expected from the preceding sections, the major change introduced by these variations on the ARDC standard is in the arrival time of the first waves. The character of the following waves is almost unchanged. The velocity range of the first arrivals is between 302 and 315 m/sec, corresponding to the arctic winter and tropical models, respectively. Excluding effects of winds, we would expect that the observed seasonal and geographic variations in arrival times of atmospheric waves would correspond to this velocity range. A rough estimate of the effect of winds will be obtained later by comparing this range with observed variations in the velocity of the first arrivals.

Vertical Distribution of Pressure and Particle Velocity

The particle velocities diverge with increasing heights in the half-space; pressure and energy converge to zero. The distribution of nodes is the same for horizontal particle velocity and

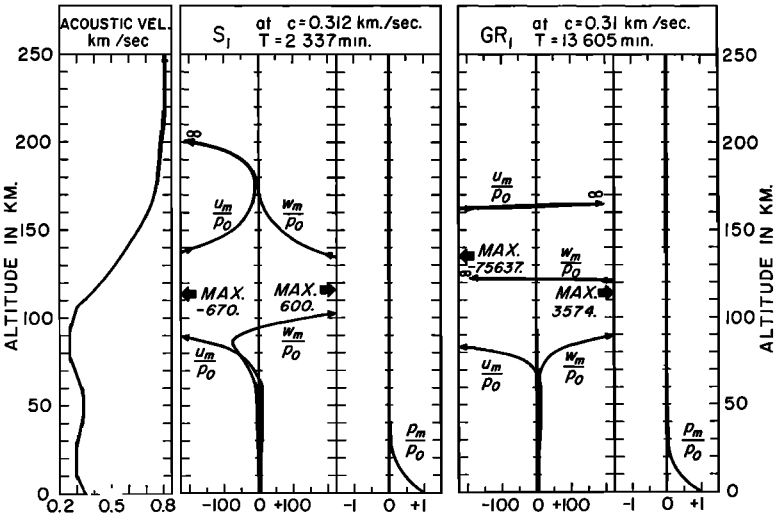

Fig. 17. Vertical distribution of normalized particle velocities and pressure for S_1 and GR_1.

pressure. The vertical distributions of these parameters normalized to surface pressure are given in Figures 16 and 17 for several modes. In general, pressure has n nodes for mode S_n, whereas vertical particle velocity has $n + 1$ nodes. For the GR_n modes, pressure has $n + 1$ nodes and vertical velocity has n nodes. Here nodes are defined as a zero value of the parameter which reverses a trend in sign which has persisted over many layers. On occasion, where near-zero values of a parameter occur, a reversal in sign may occur in association with a given layer.

Comparison with Experimental Data

Comparison in the frequency domain. Group velocities can be determined experimentally from barograms. All that is required is a knowledge of the origin time and the distance of the source. The waves A_1 travel the direct path to the detector, A_2 follow the long path through the antipodes, and A_3 represent the return of A_1 after a complete circuit of the earth.

Group velocity data are given in Figures 18 and 19, together with theoretical curves for the ARDC standard atmosphere and the two extreme cases of arctic winter and tropical atmospheres. For reasons given earlier, the data should be compared primarily with the plateaus and maximums in group velocity. Thus we would expect that the early portion of the barogram would correspond to a superposition of waves propagating according to the group velocity maximums of the GR_n and S_n modes. The group velocities labeled 1 to 8 in Figure 18 are taken from the paper by *Donn and Ewing* [1962]. These represent world-wide observations for a single explosion (Novaya Zemlya, October 30, 1961), and they indicate a geographic variation of velocity. This variation lies outside the velocity range for the extreme atmospheric models and thus supports the suggestion

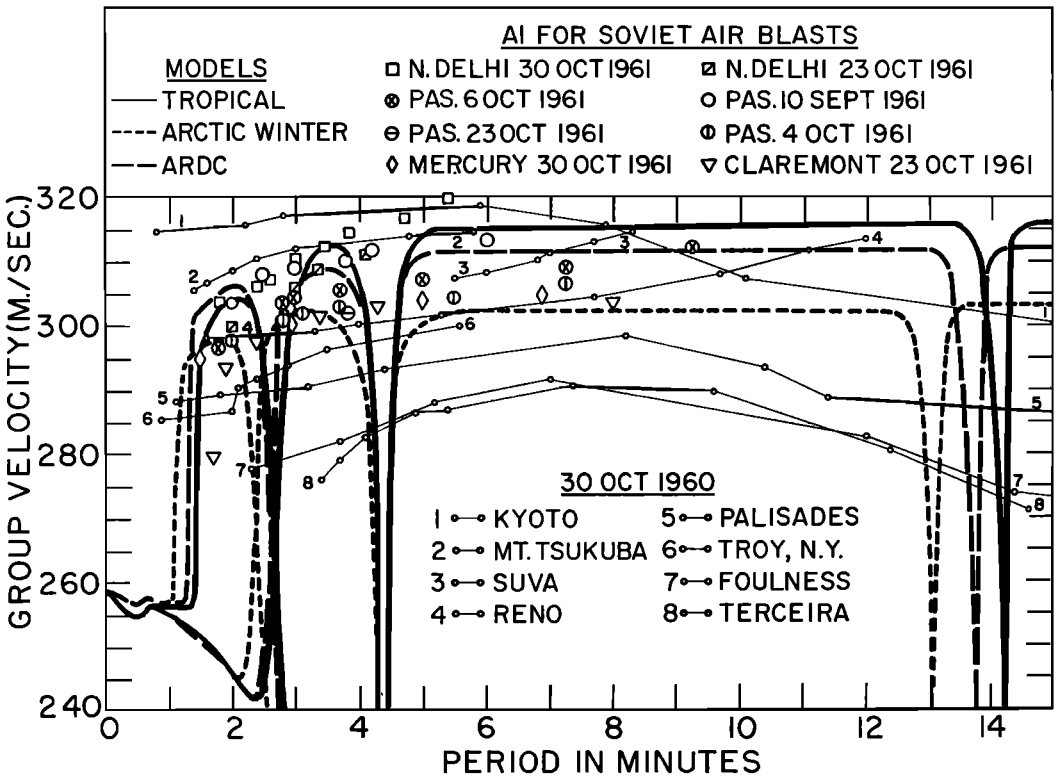

Fig. 18. Comparison of experimental group velocities for A_1 waves from Novaya Zemlya explosions with standard and extreme ARDC models. Data curves 1 to 8 from *Donn and Ewing* [1962].

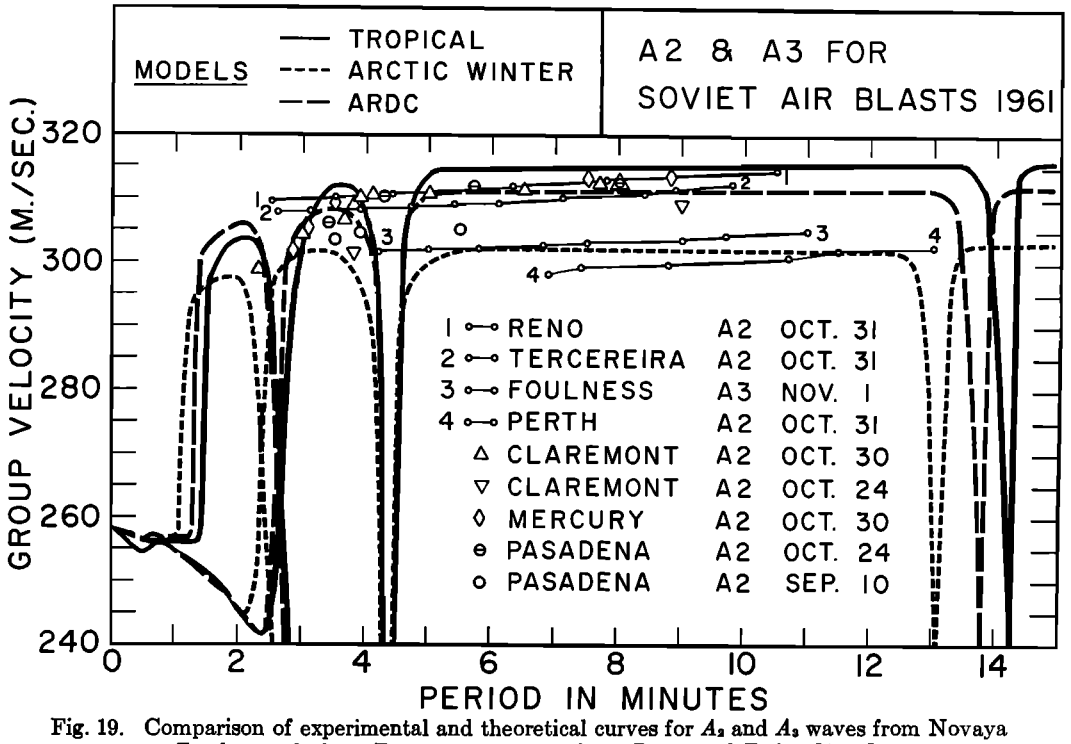

Fig. 19. Comparison of experimental and theoretical curves for A_2 and A_3 waves from Novaya Zemlya explosions. Data curves 1 to 4 from *Donn and Ewing* [1962].

of *Donn and Ewing* and of *Wexler and Hass* [1962] that winds significantly affect the propagation of A_1 waves. Donn and Ewing's data probably do not correspond to propagation according to a single mode (as these authors imply) but to superposition of modes $GR_{0,1}$, S_0, and S_1. It is not easy to separate modes when the period change between modes is small. However, several of the records published by Donn and Ewing seem to show an abrupt amplitude change that would be expected from the maximum group velocity of S_1.

Also plotted in Figure 18 are group velocity data for California and Nevada stations (Pasadena, Claremont, Mercury) for a number of Soviet explosions detonated between September 10, 1961, and October 30, 1961. These data represent almost identical paths; the variations, therefore, are indicative of atmospheric changes. Although the spread of data falls within the limits of the theoretical curves for the extreme atmospheres, we believe that this variation represents an effect of winds and not of seasonal changes in temperature. The time spread is less than two months, and the data do not show the systematic velocity decrease from September to October which would be expected were seasonal temperature changes involved.

The experimental data in Figure 19 for A_2 and A_3 waves show much less scatter. The worldwide observations of Donn and Ewing for the October 30, 1961, event (labeled 1–4) as well as the seasonal observations in southern California and Nevada for the period September 10, 1961, to October 30, 1961, fall within the range of the theoretical curves. We agree with Donn and Ewing that the reduced scatter found for A_2 and A_3 waves is a consequence of the averaging out of wind, seasonal, and geographic effects for these longer paths. The data for A_2 and A_3 plotted in Figure 19 imply that modes higher than S_0 are absent.

Donn and Ewing believe that they have observed inverse dispersion for periods longer than about 6 minutes. Waves exhibiting such dispersion would be difficult to detect, as these authors note. The details of inverse dispersion would be sensitive to the structure of the atmosphere above 100 km. Indeed, we have seen that the portions of the theoretical group ve-

locity curves corresponding to inverse dispersion differ according to the way in which the atmospheric model is terminated. Inverse dispersion data could be quite useful in resolving this problem. We take no position on the reality of the inverse dispersion data other than to note as before that the corresponding waves would probably have relatively small amplitudes for near-surface explosions and surface detectors.

Comparison in the time domain. Given phase and group velocity curves, it is possible to construct synthetic barograms for comparison with actual barograms to see if the major features of the actual barograms are explainable. Since the homogeneous wave-guide approach used in this paper does not give excitation functions, the synthetic barograms will represent only the effects of phase distortion of the wave guide.

The pressure response $p(t)$ of the atmosphere can be expressed by the Fourier integral

$$p(t) = \int_{-\infty}^{\infty} G(\omega) \exp(i\omega t)\, d\omega \qquad (30)$$

$G(\omega)$ includes the transform of the source function, the amplitude and phase response of the excitation function, and the instrumental response. We assume that $G(\omega) = F(\omega) \exp[-i\phi(\omega)]$ and that $F(\omega)$ is even in ω and has significant values in the frequency range $\omega_1 < \omega < \omega_2$. Under these conditions (30) takes the form

$$p(t) = 2\int_{\omega_1}^{\omega_2} F(\omega) \cos[\omega t - \phi(\omega)]\, d\omega \qquad (31)$$

where the phase response is $\phi(\omega) = (\omega r/c) + \phi_0$, and ϕ_0 includes instrumental phase distortion as well as initial phase of the source. *Aki* [1960] has shown how (31) can be evaluated using the approximation

$$p(t) = 2\sum_{i=1}^{n} F(\omega_i)\,\Delta\omega_i \frac{\sin\left\{\frac{\Delta\omega_i}{2}(t - t_i)\right\}}{\frac{\Delta\omega_i}{2}(t - t_i)} \cdot \cos(\omega_i t - \omega_i \tau_i) \qquad (32)$$

In this evaluation the frequency interval ω_1 to ω_2 is divided into consecutive bands $\Delta\omega_i$ with center frequency ω_i, and it is assumed that $F(\omega_i)$ is constant over the elementary bands. τ_i is the phase delay $\phi(\omega_i)/\omega_i$; $t_i = \tau_i + \omega_i (\partial\tau/\partial\omega)_i$ is the group delay. t_i is obtained from the distance, the group velocity, and the instrumental group delay.

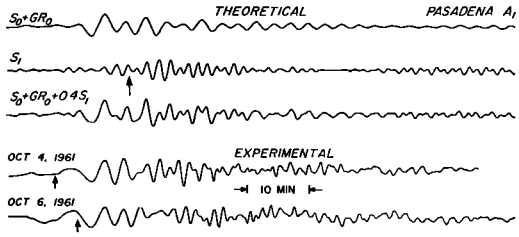

Fig. 20. Comparison of experimental and theoretical barograms of A_1 waves. Arrows show common fiducial time.

We have programmed equation 32 for computation and automatic plotting on an electronic computer. In practice we used 22 frequency bands and group delays sufficient to encompass between 1 and 2 hours of pressure-time record.

In Figure 20 the first two traces are theoretical barograms for the $(S_0 + GR_0)$ and S_1 modes, respectively, for the ARDC model terminated with the half-space at 220 km. The third trace is the sum of the first two, with the arbitrary weighting $S_0 + GR_0 + 0.4S_1$. $F(\omega_i)$ was taken to be the instrumental response in these calculations, and the excitation function was assumed to be constant over the range ω_1 to ω_2. The fourth and fifth traces are Pasadena recordings of A_1 waves from the Soviet nuclear explosions in Novaya Zemlya on October 4 and 6, 1961. The experimental and theoretical records have been aligned on the time scale for the best fit. The arrows indicate where a fiducial time would fall on each record. Comparison of the traces reveals the following: (1) The two experimental records agree in phase and group characteristics only for the first few oscillations. Thereafter they agree in group frequency only.[4] (2) The third theoretical trace roughly agrees in a similar fashion with the two experimental records, whereas the first two traces do not. From this we infer that the characteristic features of the Pasadena barogram are due to a superposition of the modes GR_0, S_0, and S_1. (3) The difference in arrival times between theoretical and experimental records is 8 minutes and 11 minutes, which times correspond to

[4] By group-frequency agreement we mean that the frequencies present at a given time are in general agreement.

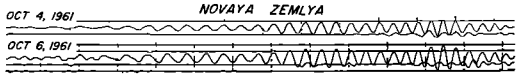

Fig. 21. Comparison of seismic surface waves recorded in Pasadena from the Soviet explosions of October 4 and 6, 1961.

discrepancies of the order of 2 to 3 per cent. Winds and the use of the standard rather than the arctic atmospheric model can account for this. The differences in the two experimental recordings for explosions separated by only two days are of interest. These differences are due to changes in the structure of the atmospheric wave guide rather than to changes in the properties of the source. This can be demonstrated by noting the complete phase and group agreement of the corresponding records of seismic surface waves from these events (Figure 21). If the atmosphere can change properties within a time interval of the order of the travel time for a complete circuit of the earth, we might expect that free oscillations of the atmosphere would be characterized by broad spectral peaks in contradistinction to the sharp peaks of the free oscillations of the solid earth.

Theoretical and experimental barograms for A_2 waves recorded in Pasadena are shown in Figure 22. In the second trace an arbitrary 12-db/octave base boost has been inserted. Only GR_0 and S_0 modes are needed in the theoretical model to give reasonably good group-frequency agreement. This suggests greater attenuation of the S_1 mode over the longer A_2 path. The arrows indicate almost perfect prediction of the arrival time.

The reasonably good agreement in general features between the actual barograms and the synthetic barograms of A_1 and A_2 on the basis of the homogeneous wave guide theory suggests to us that the primary characteristics of atmospheric waves are determined by the dispersion

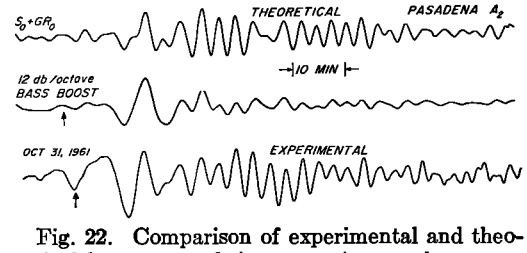

Fig. 22. Comparison of experimental and theoretical barograms of A_2 waves. Arrows show common fiducial time.

curves. In a following paper the second author will compare actual barograms with synthetic ones on the basis of the more complete inhomogeneous theory in which source and excitation functions are taken into account. Amplitude as well as group-frequency characteristics will be compared.

Appendix. List of Symbols Not Defined in Text

m, subscript indicating mth-layer constants.
α, layer sound velocity.
g, gravitational constant.
ω, angular frequency.
k, wave number in horizontal direction.
$c = \omega/k$, horizontal phase velocity.
r, horizontal cylindrical coordinate.
$\gamma = C_p/C_v$, specific heat ratio.
R^*, universal gas constant.
M_0, molecular weight at ground.
$R = R^*/M_0$.
K^*, real kinetic temperature in degrees Kelvin.
$K = (M_0/M)K^*$, molecular scale temperature.
u, horizontal particle velocity perturbation.
w, vertical particle velocity perturbation.
p, pressure perturbation.
ρ, density perturbation.
^{0}, superscript denoting the static equilibrium quantity.
z_m, the altitude at the top of the mth layer.
$d_m = z_m - z_{m-1}$, layer thickness.
t, time variable.
$T = 2\pi/kc$, period.

Acknowledgments. We are grateful to Professor Alfred B. Focke of Harvey Mudd College for making his Claremont barograms available to us; Dr. A. N. Tandon of the Government of India Meteorological Department lent us the Delhi records. The Mercury, Nevada, recordings came to us through the courtesy of Dr. J. W. Reed of the Sandia Corporation. Dr. Harry Wexler of the U. S. Weather Bureau made many materials available to us. Drs. W. Donn and M. Ewing kindly made their data available to us in advance of publication.

This research was supported by contract AF-49(638)910 of the Air Force Office of Scientific Research as part of the Advanced Research Projects Agency project Vela.

References

Aki, K., Study of earthquake mechanism by a method of phase equalization applied to Rayleigh and Love waves, *J. Geophys. Research, 68*, 729–740, 1960.

Carpenter, E. W., G. Harwood, and T. Whiteside, Microbarograph records from the Russian large nuclear explosions, *Nature, 4805,* 857, 1961.

Donn, W. L., and M. Ewing, Atmospheric waves from nuclear explosions, *J. Geophys. Research, 67,* 1855–1866, 1962.

Donn, W. L., and M. Ewing, The Soviet test of October 30, 1961, *J. Atmospheric Sciences,* in press, 1962.

Dorman, J., Period equation for waves of Rayleigh type on a layered, liquid-solid half space, *Bull. Seism. Soc. Am., 52,* 389–397, 1962.

Gazaryan, Yu. L., Infra sonic normal modes in the atmosphere, *Soviet Phys. Acoust. English Transl., 7,* 17–22, 1961.

Harkrider, D. G., and D. L. Anderson, Computation of surface wave dispersion for multilayered anisotropic media, *Bull. Seism. Soc. Am., 52,* 321–332, 1962.

Haskell, N. A., The dispersion of surface waves on multilayered media, *Bull. Seism. Soc. Am., 43,* 17–34, 1953.

Hunt, J. N., R. Palmer, and Sir William Penney, Atmospheric waves caused by large explosions, *Phil. Trans. Roy. Soc. London, A, 252,* 275–315, 1960.

Oksman, J., and E. Kataja, Round the world sound waves produced by the nuclear explosion on October 30, 1961, and their effect on the ionosphere at Sodankyla, *Nature, 4808,* 1173–1174, 1961.

Pekeris, C. L., The propagation of a pulse in the atmosphere, 2, *Phys. Rev., 73,* 145–154, 1948.

Pfeffer, R. L., and J. Zarichny, Acoustic gravity wave propagation from nuclear explosions in the earth's atmosphere, *Sci. Rept. 3, Dynamic Meteorology Project,* Lamont Geological Observatory of Columbia University, Palisades, N. Y., 1962.

Press, F., D. Harkrider, and C. A. Seafeldt, A fast, convenient program for computation of surface-wave dispersion curves on multilayered media, *Bull. Seism. Soc. Am., 51,* 495–502, 1961.

Scorer, R. S., The dispersion of a pressure pulse in the atmosphere, *Proc. Roy. Soc. London, A, 201,* 137–157, 1950.

Tolstoy, I., Modes, rays, and travel times, *J. Geophys. Research, 64,* 815–821, 1959.

Wares, G. W., K. W. Champion, H. L. Pond, and A. E. Cole, Model atmospheres, *Handbook of Geophysics,* 1-1–1-37, The Macmillan Co., 1960.

Wexler, H., and W. A. Hass, Global atmospheric pressure effects of the October 30, 1961, explosion, *J. Geophys. Research, 67,* 3875–3887, 1962.

Weston, V. H., The pressure pulse produced by a large explosion in the atmosphere, *Can. J. Phys., 39,* 993–1009, 1961.

Wilkes, M. V., *Oscillations of the Earth's Atmosphere,* Cambridge University Press, London, 1949.

Yamomoto, R., The microbarographic oscillations produced by the explosions of hydrogen bombs in the Marshall Islands, *Bull. Am. Meteorol. Soc., 37,* 406, 1956.

Yamomoto, R., A dynamical theory of the microbarographic oscillations produced by the explosions of hydrogen bombs, *J. Meteorol. Soc. Japan, 35,* 32, 1957.

(Manuscript received May 25, 1962.)